

On-Chip Controlled Surfactant–DNA Coil–Globule Transition by Rapid Solvent Exchange Using Hydrodynamic Flow Focusing

Ciprian Iliescu,*† Cătălin Mărculescu,‡ Shrinivas Venkataraman,† Baptiste Languille,§ Hanry Yu,†,||,⊥,# and Guillaume Tresset*,§

†Institute of Bioengineering and Nanotechnology, 31 Biopolis Way, The Nanos #04-01, Singapore 138669, Singapore

‡National Institute for Research and Development in Microtechnologies, IMT-Bucharest, Bucharest 077190, Romania

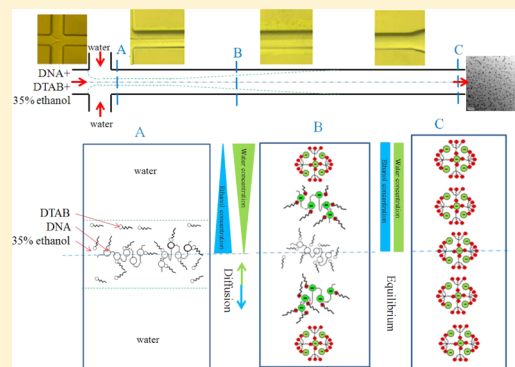
§Laboratoire de Physique des Solides, Université Paris-Sud, CNRS, 91400 Orsay, France

||Department of Physiology, Yong Loo Lin School of Medicine, National University of Singapore, Singapore 119077, Singapore

⊥Singapore-MIT Alliance for Research and Technology, 65 Nanyang Dr, Singapore 637460, Singapore

#Mechanobiology Institute, National University of Singapore, Singapore 119077, Singapore

ABSTRACT: This paper presents a microfluidic method for precise control of the size and polydispersity of surfactant–DNA nanoparticles. A mixture of surfactant and DNA dispersed in 35% ethanol is focused between two streams of pure water in a microfluidic channel. As a result, a rapid change of solvent quality takes place in the central stream, and the surfactant-bound DNA molecules undergo a fast coil–globule transition. By adjusting the concentrations of DNA and surfactant, fine-tuning of the nanoparticle size, down to a hydrodynamic diameter of 70 nm with a polydispersity index below 0.2, can be achieved with a good reproducibility.



INTRODUCTION

Recent developments in molecular biology and genomic research have given a detailed characterization of genetic diseases such as Alzheimer's, Parkinson's, and Huntington's. Gene therapy, the transfection of therapeutic genes into cells, offers the opportunity to treat, prevent, and control such diseases. Despite the ethical debate regarding the use of gene therapy in medical practice,¹ the main challenges in gene therapy are related to cell targeting, transfection efficiency, gene expression regulation, and safety issues related to gene carriers.² Current research on gene delivery vector development focuses on two major directions: viral and synthetic vectors. The use of viral vectors have recorded some successful clinical trials,^{3,4} but side effects such as immunogenic response⁵ or vector-induced cancer⁶ have limited so far the development of this method. Nonviral vectors such as lipid-based containers,⁷ inorganic nanoparticles,⁸ and polymer-based carriers^{9,10} confer advantages in terms of simplicity of use, structural and chemical flexibility in exerting control over physical and chemical properties, feasibility of large-scale production, lack of specific immune response, and a larger gene-loading capacity.^{1,9} The "synthetic solutions" must protect the DNA from intracellular and extracellular degradation,^{10,11} neutralize the negative charges of DNA, avoid the interactions with cell surface,^{12,13} and have an appropriate size for transfection. Large vector sizes favor in vitro tests due to their sedimentation to the bottom of the cell culture dish and at the same time exhibit a high

transfection efficiency; however, *in vivo*, their effect is irrelevant because either they are easily captured and degraded by the immune system or they cannot diffuse efficiently through tissues toward target cells.¹⁴ It was demonstrated for example that particles with hydrodynamic radii over 200 nm typically exhibit a more rapid rate of blood clearance than particles with radii under 200 nm and are mostly sequestered in the spleen and liver.¹⁵ Likewise, a low value of the polydispersity index (PDI) of the nanocarriers can play an important role in achieving good transfection efficiencies because the entirety of a monodisperse population of nanocarriers can potentially reach target cells, whereas the largest species of a polydisperse population are blocked by the host body thus lowering the overall transfection efficiency. In addition, the size distribution of polydisperse populations can be distorted from batch to batch which leads to a poor repeatability of the results.

Three main strategies are currently used in nonviral gene delivery: encapsulation,¹⁶ adsorption,¹⁷ and condensation.^{18,19} The encapsulation method consists of trapping DNA molecules inside biodegradable spherical micro- or nanoparticles. The method involves high shear stress or relatively high temperature that can degrade the DNA.^{8,20} The adsorption method relies on electrostatic binding of DNA molecules on biodegradable or inorganic particles; in these conditions DNA is exposed to

Received: April 11, 2014

Published: October 29, 2014



ACS Publications

© 2014 American Chemical Society

13125

dx.doi.org/10.1021/la5035382 | Langmuir 2014, 30, 13125–13136

enzymatic degradation.^{8,21} The condensation of anionic DNA by a cationic surfactant leads to a partial collapse of the DNA chains.²² In general, the size of the resulting particle is poorly controlled because the assembly process is driven by kinetics and the system quickly becomes trapped into a metastable state.

Microfluidic platforms can play an important role in the development of gene therapy and nanomedicine.^{23,24} These platforms can be used for both screening nanocarriers libraries (through *in vitro* systems mimicking *in vivo* conditions)^{25,26} and/or for the synthesis of nanocarriers with an excellent control on their size distribution, composition and morphology.²⁷ Recent works are related to the synthesis of multilayered polyelectrolyte nanocarriers as reported by Qi et al.²⁸ or assembly of lipid nanoparticles by rapid mixing in serpentine microchannels.²⁹ Kim et al. reported the processing of lipid-polymer hybrid nanoparticles (in the range 30–170 nm) using a pattern-tunable microvortex platform.³⁰ In a recent work, the same group proposed a microfluidic “factory” for single step synthesis of high-density lipoprotein with opportunity for encapsulation of hydrophobic drugs as well as quantum dots for bioimaging applications.³¹ Other important achievements are related to liposome-hydrogel hybrid nanoparticles,³² formation of lipid vesicles,^{33,34} cross-linked alginate nanoparticles,³⁵ chitosan-based nanoparticles,^{36,37} and diblock copolymers nanoparticles.³⁸ The most simple microfluidic method for achieving a precise control of the nanoparticle synthesis using diffusion-mixing process of miscible liquids is hydrodynamic flow focusing.^{39,40} In our previous work,⁴¹ we used hydrodynamic flow focusing in order to get a controlled mixing kinetics and a uniform distribution of charges at the mixing interface between polyelectrolyte (sodium carboxymethylcellulose; carboxyMC) and surfactant (dodecyl trimethylammonium bromide; DTAB) streams. The results showed a well-controlled and tunable nanoparticle size with a small polydispersity. A condition for an effective control is that the mixing time τ_{mix} be shorter than the adsorption time τ_{ad} over which the surfactant-polyelectrolyte association takes place. In other words, surfactant and polyelectrolyte must be dispersed homogeneously in the solution before they bind to each other. Unfortunately, for the compaction of DNA by surfactant, large sizes of nanoparticles with broad distributions were achieved, similar to what is obtained by mixing in bulk. These poor results may be due to an adsorption time τ_{ad} of surfactants onto DNA shorter than onto carboxyMC used previously, whereas τ_{mix} is limited by the diffusion of surfactants in both cases and is thereby unchanged. Indeed, the linear charge density of DNA is more than twice as high (5.9 e⁻/nm) as that of carboxyMC (2.5 e⁻/nm), which, in the same ionic conditions, lowers significantly τ_{ad} . Consequently, if the mixing time τ_{mix} required to homogenize DNA and surfactants is not reduced below their adsorption time τ_{ad} , the association process gives rise to large nanoparticles with uncontrolled size distribution. The mechanism is reminiscent of the self-assembly of block copolymer nanoparticles by rapid change of solvent quality: when τ_{mix} is below τ_{agg} , the nanoparticle size remains unchanged at a minimum value, whereas above τ_{agg} , the size increases as a power law of τ_{mix}^{42} .

Here, we report the use of microfluidic hydrodynamic flow focusing to enable an accurate control over the size distribution of surfactant–DNA nanoparticles by a rapid change of solvent quality. Indeed, rather than trying to further reduce the mixing time between DNA and surfactant, which is quite challenging with large molecules, we opted for a solvent exchange. It should

be noted here that we were primarily interested in long DNA chains, i.e. ~2000 base pairs which is the typical size of a gene. The compaction of short oligonucleotides such as silencing RNA (~20 base pairs) into small monodisperse nanoparticles is easier and does not require a sophisticated mixing strategy. The chosen surfactant was again DTAB because it is a chemically simple, well-established, and thoroughly documented cationic surfactant model. Upon bulk mixing, DNA collapses in a noncontrolled manner with local excess concentrations yielding large aggregates non suitable for efficient gene delivery applications. In 35% ethanol, however, DNA, and nucleic acids in general, as well as surfactant are soluble, and surfactant molecules are weakly bound to DNA chains through electrostatic interactions but do not form compact globules.⁴³ Given the small sizes of solvent molecules and their subsequent large diffusion coefficients ($\sim 10^{-9} \text{ m}^2 \text{ s}^{-1}$), the solvent quality can be changed rapidly in such a way that the surfactant-bound DNA chains collapse due to the poor solubility of the hydrocarbon chains of surfactants without having enough time to aggregate with each other by diffusion; they thereby form nearly monomolecular DNA-based nanoparticles. Compared to previous studies reporting monomolecular DNA-based nanoparticles,¹⁴ the microfluidics approach avoids resorting to chemical additives or harsh formulation processes. Besides, it offers a greater versatility than bulk synthesis, and it will enable us to finely tune the sequential assembly of multicomponent soft nanoparticles.

EXPERIMENTAL SECTION

Reagents. Dodecyl trimethylammonium bromide (DTAB) and cetyltrimethylammonium bromide (CTAB) were purchased from Sigma-Aldrich with a purity >99%. DTAB and CTAB were dissolved in Millipore Milli-Q deionized water (conductivity $<10^{-6} \text{ S m}^{-1}$) at a stock concentration of 20 mM. The critical micelle concentration for DTAB in pure water is 15 mM and therefore micelles could not be formed in any of our experiments involving DTAB. The critical micelle concentration for CTAB in pure water is 1 mM. Calf thymus DNA and λ -DNA were purchased from Invitrogen. Unless otherwise stated in the text, calf thymus DNA was always used for the experiments. The mixing of surfactant, DNA and 35% ethanol at the desired concentration was performed within 5–10 min before each experiment. Bulk mixing was performed under agitation with a magnetic stirrer.

Dynamic Light Scattering Measurements. The size and polydispersity of surfactant–DNA nanoparticles were measured by dynamic light scattering (DLS) using a Zetasizer model ZS-90 (Malvern Instrument, Ltd., UK). Data were collected at a back-scattering angle of 173° with temperature maintained at 25 °C. Because the final solutions of nanoparticles contained less than 5% ethanol, we set the refractive index to that of pure water at 25 °C. Size analysis was carried out by the cumulants method and the polydispersity index (PDI) was estimated accordingly. It should be noted that the size distributions returned by the Contin method always exhibited a single peak, at least for the experiments with DTAB. For each sample, three measurements were performed, each measurement being an average of ten values. The standard deviation of the hydrodynamic diameters was calculated for these three values.

Transmission Electron Microscopy (TEM). The morphologies of surfactant–DNA complexes were observed under a FEI Tecnai G2 F20 electron microscope using an acceleration voltage of 200 keV. The TEM samples were prepared by first placing a drop of surfactant–DNA complexes (4.0 μL) onto a formvar-coated 200 mesh copper grid (Ted Pella Inc., USA). After 1 min, the excess solution was wicked off by using filter paper. Then the staining agent, phosphotungstic acid solution (2% w/v in deionized water; 4.0 μL), was placed on the grid, and after 1 min, the excess solution was wicked off and the grid was left to dry under the ambient conditions.

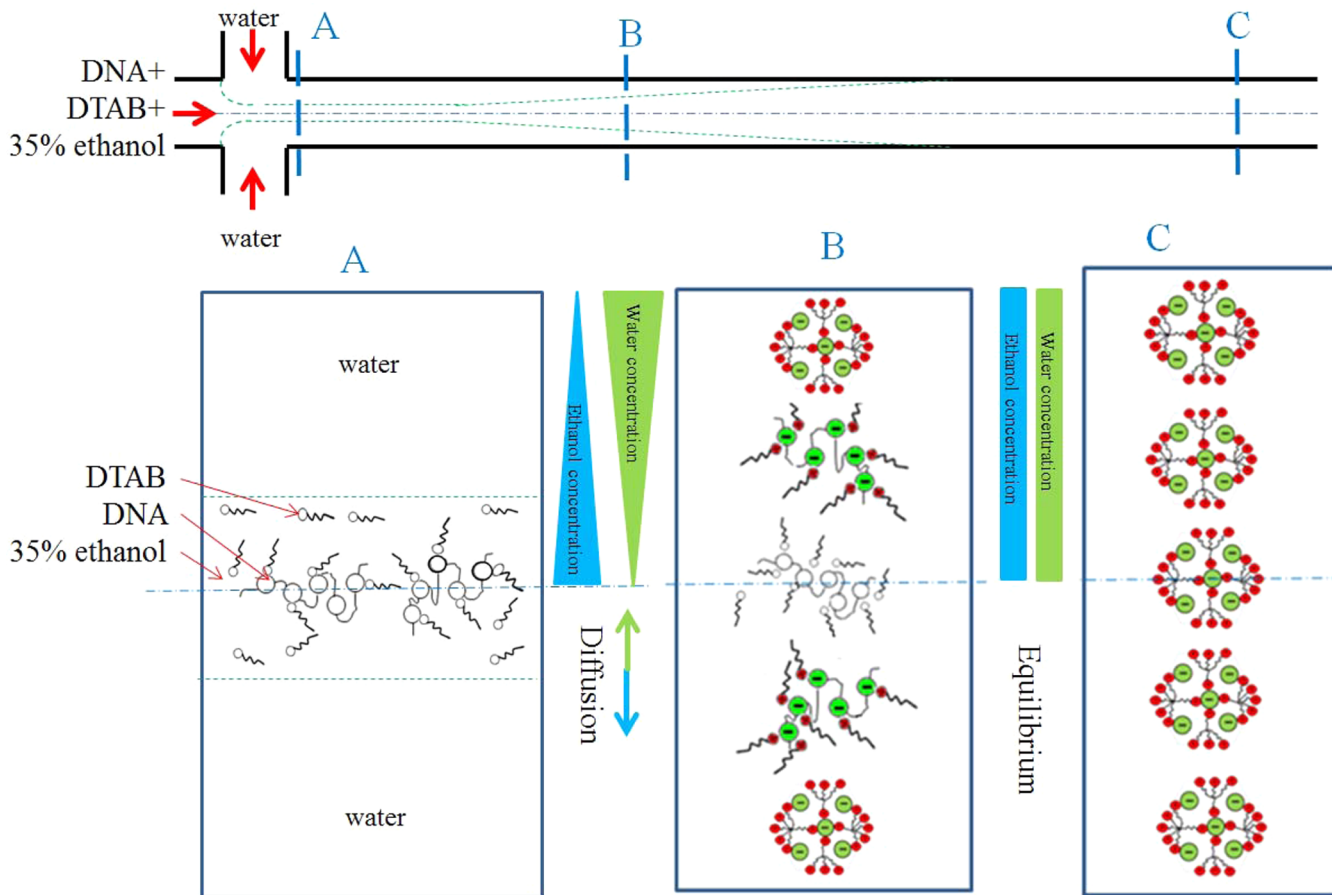


Figure 1. Rapid collapse of surfactant–DNA complexes by hydrodynamic flow focusing in microfluidic channel. A mixture of DNA, cationic surfactant (DTAB) and 35% ethanol is focused between two streams of pure water. In 35% ethanol, DTAB and DNA are weakly bound (A) and as the water content increases by transverse diffusion, the binding becomes stronger (B). At high water content, the DTAB molecules in poor solvent induce the collapse of DNA chains into nearly monomolecular nanoparticles (C).

Fabrication of the Microfluidic Device. The microfluidic channel (40- μm -depth) was fabricated in silicon using classical Deep RIE Bosch process through a 5- μm -thick photoresist, while the etch-through holes were performed using same method through a photoresist/SiO₂ mask. A 150 nm-thick dry-oxide layer was grown in a furnace on the silicon surface in order to achieve a permanent hydrophilic surface of the microfluidic channel. The silicon wafer was anodically bonded to a glass wafer for the sealing of the microfluidic channels. Finally the bonded wafers were diced in individual chips and Nanoport microfluidic connectors (Upchurch Scientific) were mounted for the inlets and outlet. Detailed considerations regarding fabrication process are presented in our previous work.⁴¹

Microfluidic Experimental Setup. A two-channel pumping system MFCS-FLEX (Fluigent, France) was used for controlling the flow of reactants through the microfluidic chip. The system was equipped with three pumping units and three flow-meters (0–50 $\mu\text{L}/\text{min}$), only two were used for the current experiment, and a software that allowed a fine-tuning of the flow rates (by varying the applied pressure) in the microfluidic device. The chip was mounted on a chip holder, and an optical microscope (Keydance) allowed the observation of the flow in the microfluidic device.

Computer Simulations. The numerical three-dimensional (3D) geometry and the structured orthogonal mesh were generated using GAMBIT preprocessor (ANSYS), consisting of 1 188 000 hexahedral finite volumes. The dimensions of the reconstructed microfluidic channel were carefully selected to capture the diffusion process with an acceptable computational cost. Therefore, the length of the inlet channels was 300 μm , the length of the outlet channel was 3000 μm , and the cross sections were 60 \times 40 μm in all cases. The 3D pressure-driven flow in the microchannel configuration was simulated using the

FLUENT CFD package (ANSYS). The code computed the isothermal laminar flows of the Newtonian working fluids, with double precision and with a 10⁻¹⁰ convergence criterion. The FLUENT code solves the Cauchy equation of motion in which the extra-stress tensor is expressed as a generalized Newtonian model:

$$\rho \left[\frac{\partial \mathbf{u}}{\partial t} + (\mathbf{u} \nabla) \mathbf{u} \right] = \rho \mathbf{b} - \nabla p + 2\nabla(\eta(\dot{\gamma})\mathbf{E}) \quad (1)$$

where ρ is the fluid density, \mathbf{b} the specific mass force, \mathbf{E} the strain rate tensor, t the time, \mathbf{u} the velocity vector, p the pressure, and η the viscosity function dependent on the shear rate $\dot{\gamma}$. All the quantities entering eq 1 varied with the position \mathbf{r} and the time t . Along with the momentum equation, the diffusion equation was also solved in order to obtain an accurate solution

$$\frac{\partial \rho(\mathbf{r}, t)}{\partial t} = \nabla [D(\rho) \nabla \rho(\mathbf{r}, t)] \quad (2)$$

where $D(\rho)$ is the collective diffusion coefficient depending on the local fluid density ρ .

The numerical simulations were performed using a Volume of Fluid method with 35% ethanol in aqueous solution ($\rho = 930 \text{ kg/m}^3$ and $\eta = 0.0011 \text{ Pa s}$) injected on the central stream and water ($\rho = 998.2 \text{ kg/m}^3$ and $\eta = 0.001003 \text{ Pa s}$) on the focusing streams. The flow rate ratio used was 5/45, considering the central streamflow rate and the sum of the focusing streams flow rates, respectively. The Reynolds numbers associated with each stream were ~ 1.5 and ~ 8.5 respectively. By using a user defined scalar (UDS), specific to the FLUENT package, we were able to activate given fluid properties such as diffusion coefficients. The UDS allowed us to customize the transport equation

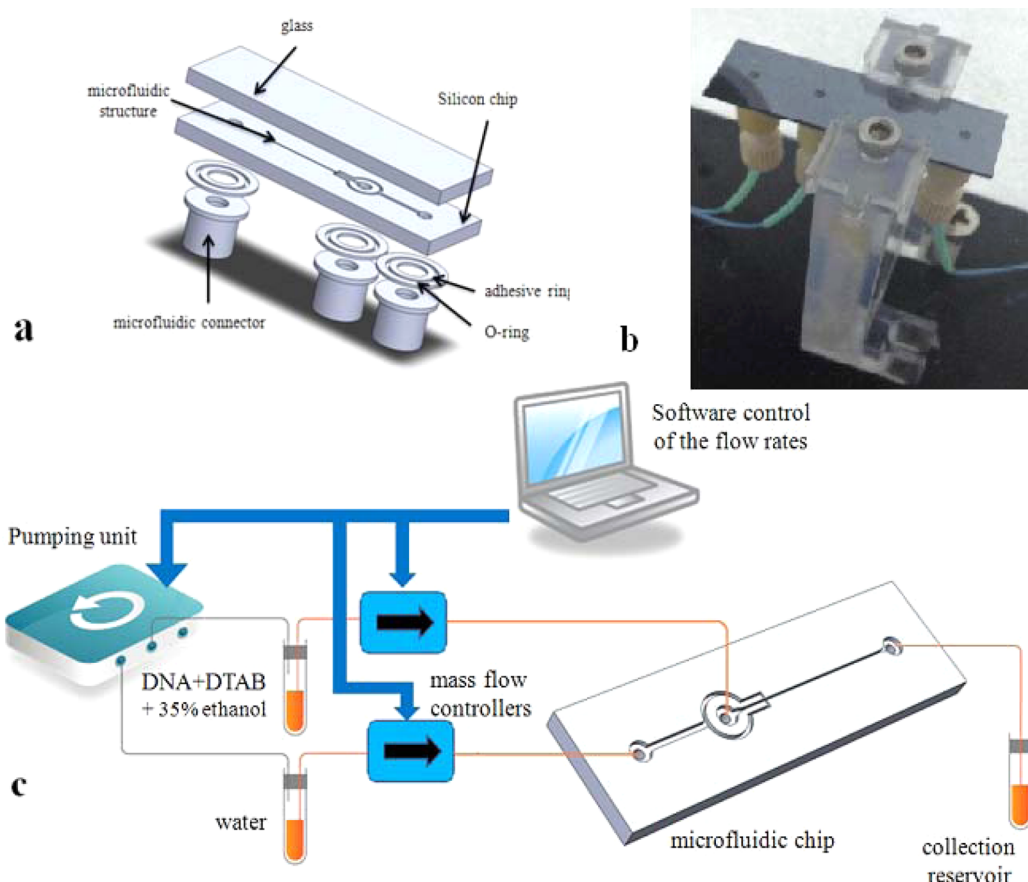


Figure 2. (a) Exploded view of the microfluidic device. (b) Optical image of the device. (c) Testing setup: two-channels MFCS-FLEX pumping unit was used for flowing the reagents and the water in a controlled manner through the microfluidic channels.

by defining solution zones, the flux function, the unsteady function and other parameters so as to obtain an accurate simulation of the diffusion process. The value for the diffusion coefficient of ethanol in water was $0.625 \times 10^{-9} \text{ m}^2/\text{s}$.⁴⁴ No chemical reaction was taken into account and the ethanol was therefore assumed to be a passive tracer in water.

RESULTS AND DISCUSSION

Working Principle. The compaction mechanism of DNA by cationic surfactant in aqueous solutions is driven by two interactions that take place almost simultaneously. The electrostatic interaction between the anionic backbone of DNA and the cationic headgroup of surfactant is supplemented by a hydrophobic interaction between the alkyl chains of the surfactant molecules.⁴⁵ As a result, the surfactant-bound DNA chains collapse (a process referred to as coil–globule transition) to form nano- or micrometer-size particles. The size of the particles is strongly dependent on the number of the DNA molecules trapped in a particle during the condensation process. Also, the presence of salt in solution favors the aggregation of particles during the course of their assembly by screening the repulsive electrostatic interactions and it generally gives rise to large particle sizes. In the present work, we propose to split the compaction process into two distinctive steps: one in bulk for the electrostatic association between DNA and surfactant and the other one on chip for the collapse of surfactant-bound DNA chains driven by the hydrophobicity of the surfactant alkyl chains in a solvent with high water content. If the solution used for solubilizing DNA and surfactant contains a high enough fraction of organic solvent such as ethanol, the alkyl chains of surfactant molecules are in a good

solvent quality and remain dissociated so that the surfactant–DNA complexes are in a coil conformation.⁴³ Note that the fraction of ethanol must be below 50% otherwise DNA precipitates. At this stage, there is only electrostatic interaction between the cationic headgroup of surfactant and the anionic backbone of DNA. This step can be easily achieved in bulk by mixing DNA and surfactant in a 35% ethanol solution. In the second step, a simple change of solvent quality through water dilution enhances the hydrophobic interactions between the alkyl chains of the surfactant molecules leading to a compaction of the surfactant–DNA complexes. Classical bulk dilution results in a poorly controlled DNA compaction, mainly due to a lack of homogeneity of molecules and charges throughout the solution yielding large aggregates and/or high polydispersity not suitable for efficient delivery applications. Forcing DNA and surfactant at high velocity into a turbulent vessel is prohibited because the high shear rates generated locally in the solution will break apart the DNA chains. A gentle method for achieving a rapid change of solvent quality involves hydrodynamic flow focusing in a microfluidic channel. When a central stream of good quality solvent is flown through a microfluidic channel and sandwiched between two side streams of pure water, its width is strongly reduced due to a focusing effect, which is possible only because of the low Reynolds number of the liquids and their subsequent laminar flow.^{46,47} The pure water diffuses transversely through the central stream (and vice versa) in a mixing time τ_{mix} all the shorter as its width is reduced and changes accordingly the solvent quality. This second step of the process developed on-chip is illustrated in

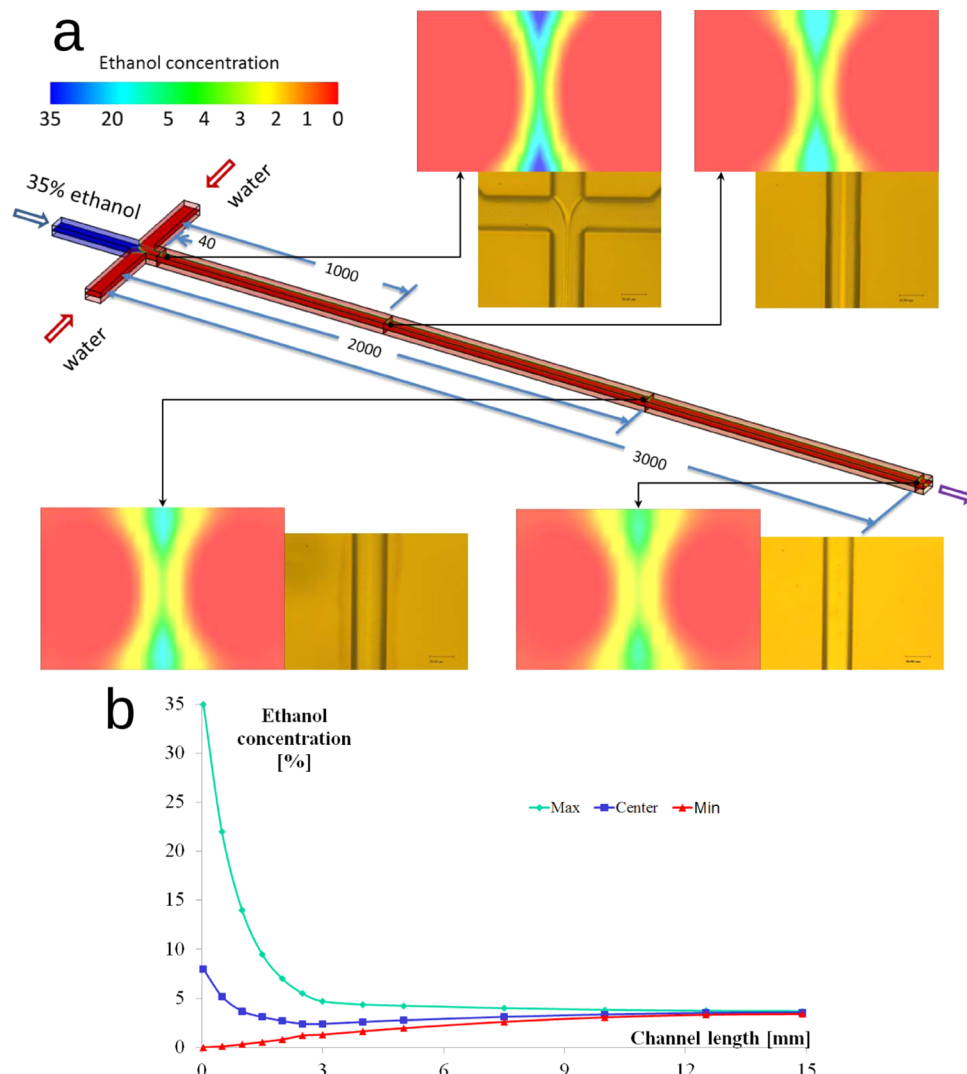


Figure 3. (a) Simulation results presenting the mixing process along the microfluidic channel: near the confluence point, and at 1, 2, and 3 mm from the focusing point. Attached to the simulated cross sections, optical images of the channel illustrate the mixing process (the width of the microfluidic channel is 60 μm). (b) Calculated variations of the ethanol concentration in cross sections (maximal value, minimal value and the value at the center of the channel) taken along the channel length. The values for channel lengths greater than 3 mm were obtained by extrapolating the simulation results with a set of exponential functions.

Figure 1. A mixture of calf thymus DNA, DTAB, and 35% ethanol flowing in the central channel is hydrodynamically focused using two streams of pure water. Near the intersection of the channels (cross-section A) the surfactant molecules are bound to the DNA chains due to electrostatic interactions but the complexes are still in a coil conformation. As a result, the diffusion starts to occur (35% ethanol in water and water in 35% ethanol), and the surfactant-bound DNA chains gradually collapse from a coil to a globule conformation. Assuming that the coil-to-globule transition takes place at the same rate as that of the solvent change, a simple requirement for obtaining nearly monomolecular nanoparticles is that the mixing time governed by the solvent diffusion be shorter than the aggregation time τ_{agg} over which the surfactant-bound DNA chains diffuse toward each other, namely $\tau_{\text{mix}} < \tau_{\text{agg}}$. Note that τ_{agg} is much larger than the adsorption time τ_{ad} defined in the introduction: τ_{agg} is limited by the slow diffusion of surfactant-bound DNA while τ_{ad} is driven by the electrostatic attraction between DNA and surfactant. In the present study, the surfactant molecules are already adsorbed on DNA from the beginning but they do

not induce a coil–globule transition thanks to the good solvent quality (35% ethanol); upon the change of solvent, the size of nanoparticles is determined by the aggregation of collapsing surfactant-bound DNA chains. At the end of the microfluidic channel, there is a uniform and low concentration of ethanol along the cross-section (cross-section C) of the channel and the surfactant–DNA coil-to-globule transition is fully completed.

Microfluidic Setup. The microfluidic setup was designed in order to ensure repeatable and controllable results (for this reason special attention was given to the microfluidic device and to its cleaning process). The microfluidic circuit, illustrated in Figure 2a, was fabricated in silicon, a glass die being bonded on top of the silicon structure. The advantage of this combination of materials lies in a very good definition of the structure of the microfluidic circuit.^{48–50} Moreover, the hydrophilic nature of the channel surface (the silicon surface was oxidized) prevented unspecific interactions with the nanoparticles. It should be noted also that since the reagents were flowing continuously at relatively high velocities, the risk of adsorption onto the channel walls was rather low. The device

could be easily cleaned after each experiment by flowing NMP (*N*-methylpyrrolidone) for 15 seconds through the central inlet. This operation was performed without any modification of the testing setup, just by simple replacement of the reservoir connected to the main channel. A buffer solution (35% ethanol) was flown (for 1 min) after NMP in order to avoid any contamination of the surfactant–DNA sample. This point is crucial not only for the accuracy of the experiments (all the experiments were performed on the same chip and in the same flowing conditions) but also for the scalability of the nanoparticle synthesis: the device can be reused and an automatic cleaning process can be setup after a certain processing time. The microfluidic chip and its fabrication process were completely described in our previous work,⁴¹ for this reason we will underline here only the main characteristics. The device presented two inlets: the central one for the DTAB/DNA/35% ethanol solution, and the other one, that assured the hydrodynamic focusing of the previously mentioned reagents, containing pure water. The water channel was divided into two symmetrical branches in order to ensure a symmetrical focusing and an identical pressure drop on the branches. The depth of the microfluidic channel was 40 μm , the width was 60 μm , while its length was 1.5 cm.⁴¹ A photograph of the microfluidic chip and its holder is presented in Figure 2b. The microfluidic setup is represented in Figure 2c, the pumping unit and mass flow controllers were software-controlled and assured a fine-tuning of the flowing parameters in the microfluidic device.

Simulation Results. Numerical simulations illustrate with accuracy the three-dimensional process of solvent homogenization while fluids are flowing through the channel. The results of the simulations as well as some optical images (top view) with the mixing process in microfluidic channel are presented in Figure 3a. For the visualization of the mixing process, four cross sections through the microfluidic channel were selected at fixed intervals. First point was selected very close to the focusing area (40 μm), and from the simulation a very strong gradient in ethanol concentration (0–35%) is observed. Also the contrast on the optical image between the central stream (ethanol) and the lateral streams is evident. Once the diffusion process started the main stream became less and less visible due to the progress in the mixing process. The maximal calculated value of ethanol concentration also decreases (from 35%, the initial value, to 14% for a channel length of 1 mm, 7% for 2 mm, and 4.7% for 3 mm). The graphical variations of the maximal and minimal calculated values of the ethanol concentration as well as the values in the center of the microfluidic channel are presented in Figure 3b. By extrapolating the numerical solution obtained over 3 mm of channel with a set of exponential functions, the curves converged to a uniform concentration (3.5% ethanol) at the end of a 15 mm-long microfluidic channel demonstrating that the mixing process was complete within the channel. The extrapolated values of the ethanol concentration close to the outlet were: maximal 3.7%, minimal 3.41%, center point 3.56%.

Analytical Considerations. Let Q_A and Q_B be the flow rates of the central and lateral streams respectively, and w_f and w_o the widths of the focused and outlet streams (Figure 4). Because the fluids are incompressible and the flows are laminar, the principle of mass conservation stipulates that flow rates are conserved along the channel, namely

$$Q_A = w_f \bar{v}_f h \quad (3)$$

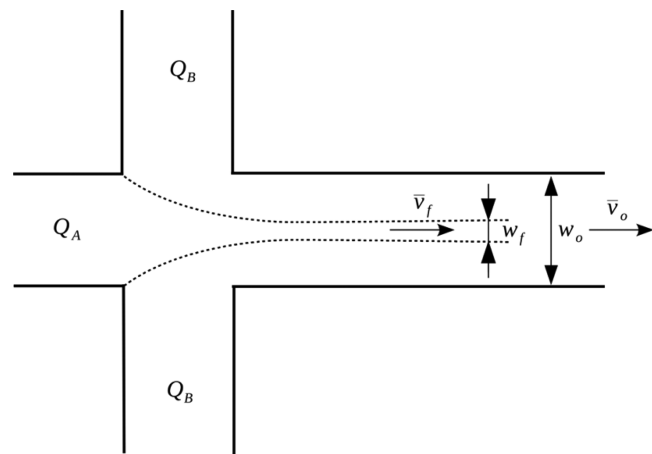


Figure 4. Schematic illustration of hydrodynamic flow focusing.

and

$$Q_A + 2Q_B = w_o \bar{v}_o h \quad (4)$$

where h denotes the height of the channel and \bar{v}_f and \bar{v}_o are the average flow velocities in the focused and outlet streams. These two equalities can be rearranged to yield an expression of the flow rate ratio $R \equiv 2Q_B/Q_A$:

$$R = \frac{1}{\gamma} \frac{w_o}{w_f} - 1 \quad (5)$$

where $\gamma \equiv \bar{v}_f/\bar{v}_o$ is a velocity ratio to be found. Equation 5 is obtained from the incompressibility of the fluids in a regime of laminar flow. As a result of the strong reduction of w_f via R , the time required for the pure water to diffuse transversely across the focused stream is considerably shortened. Since viscous effects dominate, the flow in the outlet channel can be assumed to be fully developed. In the approximation of large aspect ratio, i.e., $w_o \ll h$, and by imposing a no-slip condition on the channel wall, the longitudinal fluid velocity $v(x)$ obeys to the Poisson equation:

$$v(x) = v_{\max} \left(1 - 4 \frac{x^2}{w_o^2} \right) \quad (6)$$

where x is the transverse coordinate and v_{\max} the maximal fluid velocity at the channel center. In the limit where the width of the focused stream is small compared to the width of the channel, i.e., $w_f/w_o \ll 1$, the average flow velocity of the focused stream reads

$$\bar{v}_f = \frac{1}{w_f} \int_{-w_f/2}^{w_f/2} v(x) dx \approx v_{\max} \quad (7)$$

Similarly, $\bar{v}_o \approx (2/3)v_{\max}$ which yields $\gamma \approx 3/2$. This approximation was proven quite accurate by comparison with numerical simulations.⁴¹ The mixing time can be estimated as the time required for water molecules to transversely diffuse through the focused stream from both sides, that is, across a distance $w_f/2$. Therefore, if D_{water} is the diffusion coefficient of pure water in a mixture of water and ethanol, the mixing time τ_{mix} can be expressed by³⁸

$$\tau_{\text{mix}} = \frac{w_f^2}{4D_{\text{water}}} \approx \frac{w_o^2}{9(1+R)^2 D_{\text{water}}} \quad (8)$$

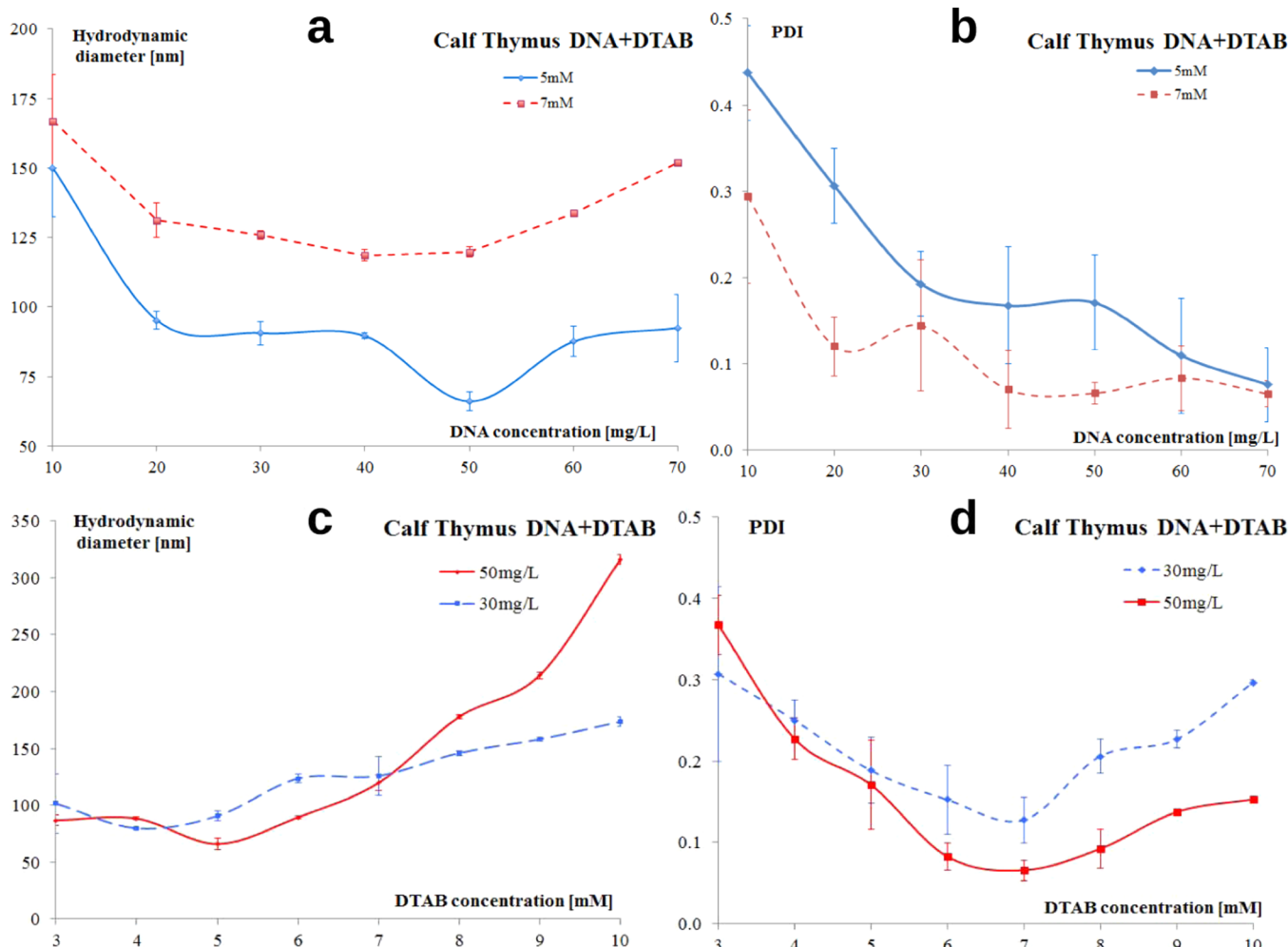


Figure 5. On-chip synthesis of DTAB/calf thymus DNA nanoparticles. The flow rate of the DTAB/DNA stream was 5 $\mu\text{L}/\text{min}$ and that of the water stream 45 $\mu\text{L}/\text{min}$. (a) Hydrodynamic diameter and (b) PDI as a function of DNA concentration for DTAB concentrations of 5 and 7 mM. (c) Hydrodynamic diameter and (d) PDI as a function of DTAB concentration for 30 and 50 mg/L of DNA.

With $D_{\text{water}} \approx 10^{-9} \text{ m}^2 \text{ s}^{-1}$, $\omega_0 = 60 \mu\text{m}$, and $R = 9$, the mixing time is 4 ms. This value must be compared to the aggregation time τ_{agg} over which two surfactant-bound DNA chains encounter each other by diffusion. As a rule of thumb, τ_{agg} can be estimated from the diffusion-limited rate constant between two uncharged surfactant-bound DNA chains such that

$$\tau_{\text{agg}}^{-1} \approx 16\pi\rho DR_h \quad (9)$$

with ρ the number density of chains which is of the order of 10^{19} m^{-3} for a concentration around 20 mg/L, D their diffusion coefficient, and R_h their hydrodynamic radius. Notice that the aggregation time given with this value of ρ is a lower bound because the chains also diffuse transversely as they travel along the channel and ρ thereby decreases by dilution. Following the Stokes-Einstein relationship, $DR_h = k_B T / 6\pi\eta$, with k_B the Boltzmann constant, T the temperature, and η the viscosity of the solvent which is $\sim 2.3 \text{ mPa s}$ for 35% ethanol at 25 °C. This yields $\tau_{\text{agg}} \approx 21 \text{ ms}$ and we are indeed in the regime where the solvent exchange occurs faster than the aggregation of surfactant-bound DNA chains, i.e., $\tau_{\text{mix}} < \tau_{\text{agg}}$.

Parameters Effect on Size and Polydispersity of Surfactant–DNA Nanoparticles. Influence of Calf Thymus DNA Concentration. The influence of DNA concentration was

studied in the range between 10 mg/L to 70 mg/L for two concentrations of surfactant, i.e. 5 mM and 7 mM. In this case the flow rate in the central stream (DTAB/DNA/35% ethanol) was kept constant at 5 $\mu\text{L}/\text{min}$ while the pure water flow rate was 45 $\mu\text{L}/\text{min}$ ($R = 9$). In this case the final concentration of ethanol in the collection reservoir was less than 4%. Figure 5a presents the variation of the hydrodynamic diameter with the DNA concentration, while Figure 5b depicts the PDI variation with DNA concentration. It can be noticed that there are three zones on the graph:

(i) A zone of low concentration of DNA (around 10 mg/L) characterized by large nanoparticle sizes and nonrepeatable results (large values of standard deviation and PDI). It was expected that, in the initial solution, each negative charge from the DNA chain to be neutralized by the positive charge of the surfactant. During the compaction process, the presence of a large number of surfactant molecules in the solution could enhance the adsorption of more surfactant molecules in the final nanoparticles due to the hydrophobic interactions between alkyl chains. DNA might thus behave as a heterogeneous nucleus that lowers the activation energy barrier to surfactant-surfactant association.

(ii) Equilibrium zone: the optimal ratio between the positive charges and the negative charges (the system was always above

the isoelectric point because the surfactants carrying positive charges were in excess. Note that for 5 mM DTAB, 1.65 g/L of DNA were necessary to achieve neutralization). It is interesting to observe that the hydrodynamic diameter of the particles with DNA concentration did not vary much for DNA concentrations between 20 mg/L up to 60 mg/L. For the concentration of surfactant of 5 mM, it could be noticed an optimum point in DNA concentration (50 mg/L) where the hydrodynamic diameter of the nanoparticles was below 70 nm.

(iii) High concentration of DNA: the size of the nanoparticles started to slowly increase. The increase of the hydrodynamic diameter in this zone can be explained by the presence of multiple DNA chains inside a single nanoparticle. According to eq 9, $\tau_{\text{agg}} \propto \rho^{-1}$; therefore, a higher DNA concentration lowers the aggregation time. We then arrived at an aggregation time comparable to or smaller than the mixing time ($\tau_{\text{mix}} \approx \tau_{\text{agg}}$) and the surfactant-bound DNA chains could aggregate during the solvent exchange. It is important to notice that the PDI decreased with the increase of DNA concentration. A value of DNA concentration between 30 to 70 mg/L is then recommended for achieving uniform and well-controlled surfactant–DNA nanoparticles.

Influence of Surfactant (DTAB) Concentration. The variation of the hydrodynamic diameter of the nanoparticles with the surfactant concentration was studied for DTAB concentrations between 3 mM and 10 mM, for two values of DNA concentration: 30 and 50 mg/L. Figure 5c,d illustrates the influence of DNA concentration on the hydrodynamic diameter of the nanoparticles and PDI, respectively. The graph presented in Figure 5c shows the same trend as the graph representing the influence of DNA concentration. Both curves present a minimum value. The low DNA concentration zone from the graph presented in Figure 5a has a correspondence in Figure 5c in the area with high surfactant concentration, while the area with high concentration of DNA from Figure 5a is similar to the area with low surfactant concentration. This aspect was somehow expected, the ratio between positive and negative charges playing an important role in the compaction of DNA. It must be mentioned that 3 mM was a limit for the concentration of the surfactant (the results presented a large value of PDI), also for large values of DTAB concentration (9 mM and 10 mM), the size of the nanoparticles started to increase as well as PDI. We can conclude that values of DTAB concentration of 5 mM up to 8 mM are the most recommended for tuning the size of nanoparticles while keeping a reasonable polydispersity (PDI below 0.2).

Influence of Flow Rate Ratio. For the influence of the flow rate ratio on the hydrodynamic diameter and polydispersity, we compared the nanoparticle sizes obtained by on-chip and bulk mixing. To do so, we used 50 mg/L of calf thymus DNA and 6.5 mM of DTAB in 35% ethanol. The flow rate of pure water was controlled between 40 and 45 $\mu\text{L}/\text{min}$ while the flow rate of the DTAB/DNA/35% ethanol solution was varied between 1 and 10 $\mu\text{L}/\text{min}$. The results are presented in Table 1. Strikingly, the nanoparticles were much larger and more polydisperse when prepared by bulk mixing than by on-chip mixing for the same final concentrations of DNA and DTAB. The batch-to-batch reproducibility was also less good. Besides, it can be noticed that there was no significant influence of the flow rate ratio when $R \geq 7.5$. The change of solvent quality took place over a time τ_{mix} smaller than the aggregation time, i.e., $\tau_{\text{mix}} < \tau_{\text{agg}}$ whatever the flow rate ratio: τ_{mix} was estimated to be 5.5 and 0.189 ms for $R = 7.5$ and 45, respectively, while τ_{agg}

Table 1. Influence of the Flow Rate Ratio R on the Size (i.e., the Hydrodynamic Diameter) of the Surfactant–DNA Nanoparticles Obtained by on-Chip and Bulk Mixing^a

flow rate ratio DNA +DTAB/water [$\mu\text{L}/\text{min}$ / $\mu\text{L}/\text{min}$] (R)	size [nm]		STDEV ^b [nm]		PDI ^c	
	on-chip	bulk	on-chip	bulk	on-chip	bulk
1/45 (45)	107	528	3.50	101	0.18	0.45
2/45 (22.5)	102	364	1.08	137	0.18	0.42
3/45 (15)	103	147	0.25	39	0.21	0.43
4/45 (11.25)	103	283	2.89	71	0.21	0.43
5/45 (9)	97	433	1.53	20	0.16	0.44
6/45 (7.5)	100	178	2.80	5.2	0.17	0.45
9/45 (5)	200	199	33.64	21	0.38	0.32
10/40 (4)	210	288	6.8	81	0.38	0.35

^aDNA and DTAB initial concentrations were 50 mg/L and 6.5 mM respectively. ^bSTDEV = standard deviation. ^cPDI = polydispersity index.

was around 9 ms for the DNA concentration considered here. As such, the kinetics of nanoparticle formation was governed solely by the collapse of surfactant-bound DNA chains. Therefore, the hydrodynamic diameter of the resulting nanoparticles was only a function of the concentrations of DTAB and DNA and hardly depended on the flowing condition. This finding is opposite to the results from our previous work⁴¹ where the flowing conditions played an important role on the hydrodynamic diameter of the nanoparticles. Indeed, the mixing time was limited by the diffusion of reagents, surfactant and polyelectrolyte, whereas in the present study, it relied on the diffusion coefficient of the solvent which was one or two orders of magnitude higher than that of the reagents due to the small size of the solvent molecules. In our previous work, τ_{mix} was thus greater or comparable to τ_{ad} and as a consequence, the final nanoparticles were dependent on the mixing kinetics, i.e., on the flow rate ratio between the streams carrying both reagents. Such a situation was observed in the present study when $R \leq 5$ (see Table 1): for example, at $R = 5$, τ_{mix} was estimated to be 11 ms, that is, slightly larger than an estimated τ_{agg} of 9 ms. As a consequence, the nanoparticle size increased to 200 nm simply because the assembly started to depend on the mixing kinetics.

Influence of the Lengths of Surfactant and DNA. In order to assess the influence of surfactant, we used cetyltrimethylammonium bromide (CTAB) in lieu of DTAB. CTAB has a longer alkyl chain (16 carbons) than DTAB (12 carbons), and consequently, its critical micelle concentration is lower (1 mM) than that of DTAB (15 mM). CTAB is also known to form cylindrical micelles above its critical micelle concentration. Figure 6 presents the results obtained with CTAB and calf thymus DNA at a flow rate ratio $R = 9$ as in Figure 5. We can see that the DNA concentrations were one order of magnitude lower than the DNA concentrations used in Figure 5. Moreover, the nanoparticle sizes were all greater than 100 nm and PDI was always above 0.15. Because the critical micelle concentration of CTAB in pure water is very low, we can expect that, in 35% ethanol, a high number of CTAB molecules were bound to the DNA chains due to the strong attraction occurring between the CTAB alkyl chains. After the on-chip change of solvent quality, the resulting nanoparticles had thereby a larger size and a broader distribution than with DTAB.

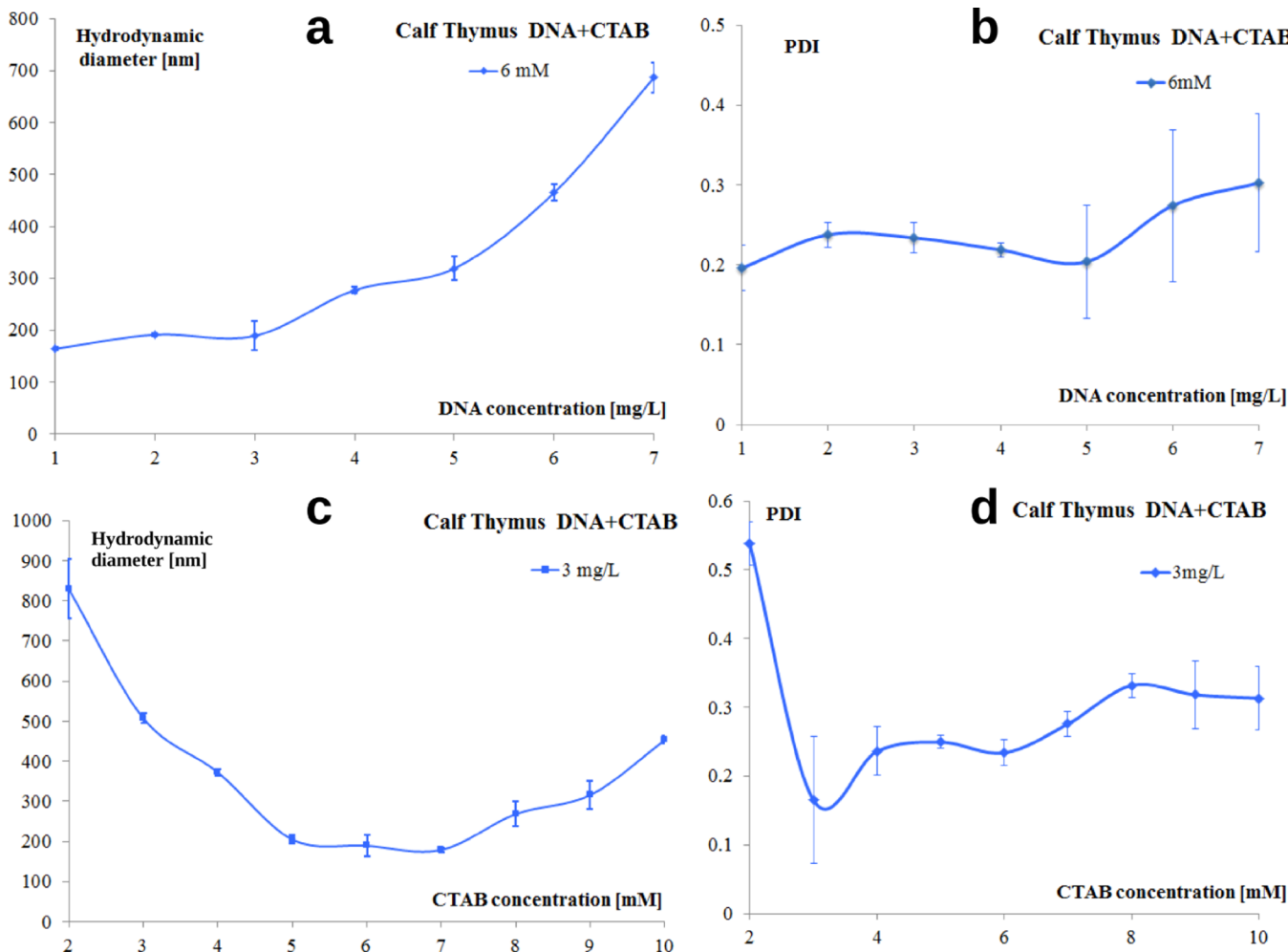


Figure 6. On-chip synthesis of CTAB/calf thymus DNA nanoparticles. The flow rate of the CTAB/DNA stream was 5 $\mu\text{L}/\text{min}$ and that of the water stream 45 $\mu\text{L}/\text{min}$. (a) Hydrodynamic diameter and (b) PDI as a function of DNA concentration for a CTAB concentration of 6 mM. (c) Hydrodynamic diameter and (d) PDI as a function of CTAB concentration for 3 mg/L of DNA.

In another series of experiments, we replaced calf thymus DNA (< 2 kbp) by λ -DNA (~48 kbp) which is at least 24-fold longer. The surfactant was DTAB and the synthesis was carried out at a flow rate ratio $R = 9$ as usual. Quite surprisingly, the λ -DNA concentration that yielded the smallest sizes was more than one order of magnitude lower than with calf thymus DNA (Figure 7), whereas the aggregation time τ_{agg} should not depend on the DNA size. However, the aggregation time given by eq 9 holds if the surfactant-bound DNA chains do not interact with each other, which might be not the case with λ -DNA in salt-free solvent. As a consequence, we had to work at very low λ -DNA concentrations so as to be in a dilute regime. The variations of the hydrodynamic diameters and PDI in Figure 7 are similar to those in Figure 5 except that the values are all higher in the former case: the mechanisms of nanoparticle assembly were therefore the same but the DNA concentrations were shifted to low values. Moreover, given that λ -DNA was very long, the nanoparticles were bigger and their polydispersity was necessarily larger because the addition of a single λ -DNA chain into a nanoparticle gave rise to a large increase in size.

TEM Images. Surfactant–DNA nanoparticles obtained by hydrodynamic flow focusing were imaged using transmission electron microscopy (TEM) with phosphotungstic acid as

staining agent. The concentration of DTAB was 5 mM while the concentration of DNA was 50 mg/L. The PDI measured by DLS for such conditions was 0.18, which means a relative standard deviation of 42% on the nanoparticle size distribution; despite the lack of accuracy, TEM images seem consistent with this value. The diameters of the nanoparticles were found to be ~30 nm by TEM (Figure 8). Compared to the hydrodynamic diameter of the nanoparticles measured by DLS (~70 nm), these values were smaller. This discrepancy in the particle size, as measured by DLS and TEM could be primarily due to inherent differences in the sample states for these respective techniques. For DLS measurements, surfactant–DNA nanoparticles were measured in their native hydrated state, as obtained from the microfluidic device. However, for the TEM measurements, the samples were observed in dehydrated state under high vacuum. Such changes in the sample state could contribute toward shrinking. Moreover, the hydrodynamic diameters measured by DLS include a hydration layer and therefore always overestimate the real size of particles. Chittimalla and co-workers reported a size of ~30 nm for surfactant–DNA nanoparticles and they estimated that each nanoparticle contained a single DNA molecule.¹⁴ Since the DNA used was about twice as long as ours, we can reasonably

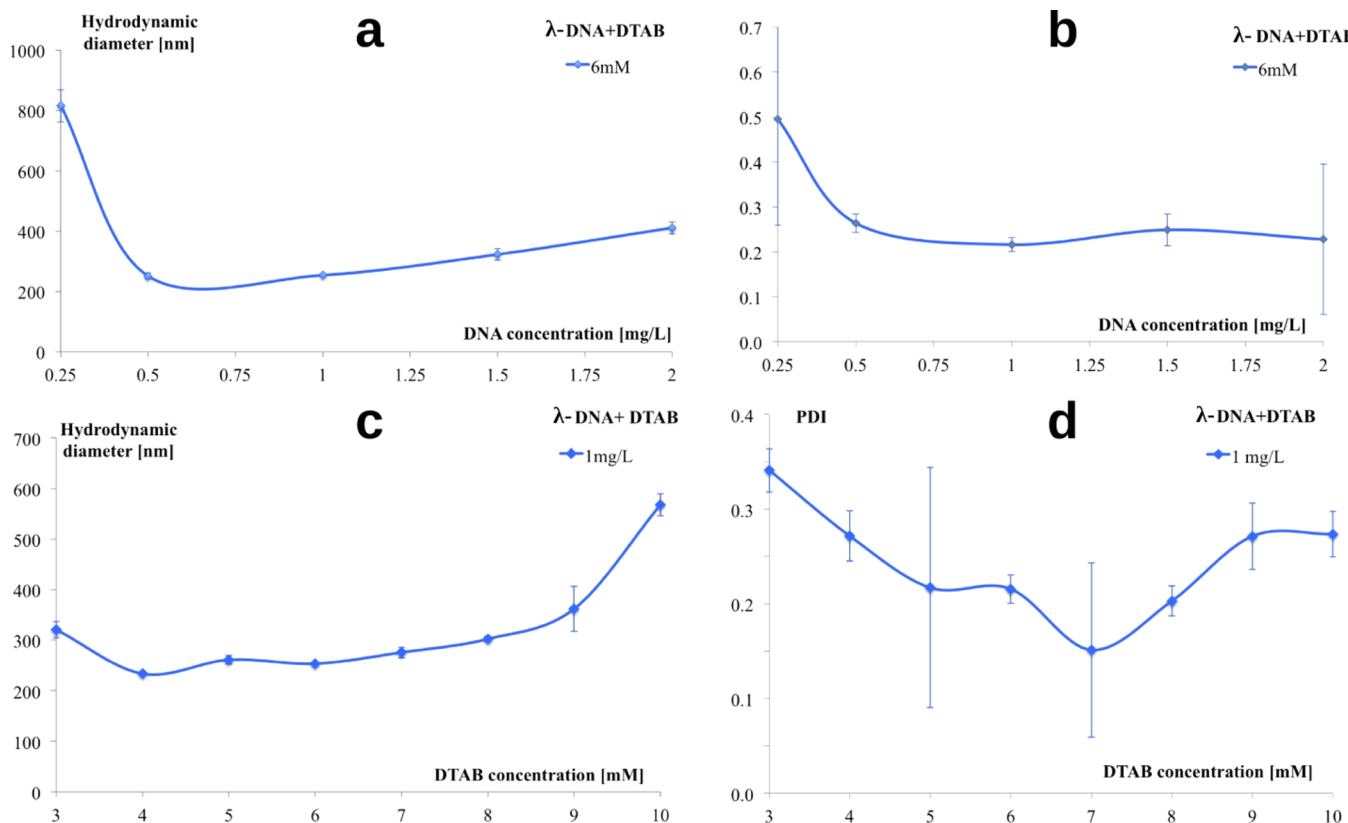


Figure 7. On-chip synthesis of DTAB/λ-DNA nanoparticles. The flow rate of the DTAB/λ-DNA stream was 5 μL/min and that of the water stream 45 μL/min. (a) Hydrodynamic diameter and (b) PDI as a function of λ-DNA concentration for a DTAB concentration of 6 mM. (c) Hydrodynamic diameter and (d) PDI as a function of DTAB concentration for 1 mg/L of λ-DNA.

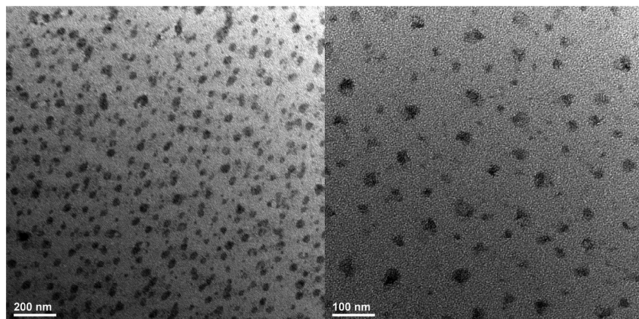


Figure 8. TEM images of DTAB/calf thymus DNA nanoparticles obtained by hydrodynamic focusing. The concentration of DTAB was 5 mM while the concentration of DNA was 50 mg/L. The hydrodynamic diameter of the nanoparticles (measured by using DLS) was 70 nm.

estimate that our smallest nanoparticles contained 2 or 3 DNA chains at most and were therefore nearly monomolecular.

CONCLUSIONS

In this report we successfully demonstrated the use of a microfluidic hydrodynamic flow focusing device in combination with an on-chip rapid solvent quality change strategy, to yield well-defined surfactant–DNA nanoparticles with excellent control over their hydrodynamic diameter (~70 nm) and distribution (PDI < 0.2). Straightforward and accurate control on the morphological properties of surfactant–DNA nanoparticles may have broad implications in gene delivery: it may enhance the bioavailability of the delivery vectors and offer a

good batch-to-batch reproducibility that could enable screening and optimization of libraries of nanoparticles in order to identify superior formulations. Also, small nanoparticles exhibit good *in vivo* circulatory properties and extended lifetime in the bloodstream.¹⁴ Our approach in principle could also be extended to the synthesis of other soft nanoparticles based on electrostatic interactions including lipid- and peptide-based delivery systems as well as complexes of polyelectrolytes used in colloidal industry.

AUTHOR INFORMATION

Corresponding Authors

*E-mail: ciliescu@ibn.a-star.edu.sg. Tel: +65 6824 7137.

*E-mail: guillaume.tresset@u-psud.fr. Tel: +33 1 69 15 53 60.

Notes

The authors declare no competing financial interest.

ACKNOWLEDGMENTS

The authors thank Mehdi Zeghal for performing measurements of diffusion coefficients by pulsed-field gradient NMR as well as Anniina Salonen and Ming Ni for stimulating discussions. This research was supported by the Institute of Bioengineering and Nanotechnology (Biomedical Research Council, Agency for Science, Technology, and Research, Singapore) (C.I., S.V., and H.Y.), and partially by the France-Singapore Merlion Program (Project Reference 8.02.10), and by CNRS through the “Interface Physique, Chimie, Biologie” program (G.T.). C.M. acknowledges support from the contract O2.1.2, no.209, ID 665.

■ REFERENCES

- (1) Niidome, T.; Huang, L. Gene therapy progress and prospects: nonviral vectors. *Gene Ther.* **2002**, *9*, 1647–1652.
- (2) Lin, Y.; Zhang, Y.; Qiao, Y.; Huang, J.; Xu, B. Light and host-guest inclusion mediated salmon sperm DNA/surfactant interactions. *J. Colloid Interface Sci.* **2011**, *362*, 430–438.
- (3) Kay, M. A.; Manno, C. S.; Ragni, M. V.; Larson, P. J.; Couto, L. B.; McClelland, A.; Glader, B.; Chew, A. J. Evidence for gene transfer and expression of factor IX in haemophilia B patients treated with an AAV vector. *Nat. Genet.* **2000**, *24*, 257–261.
- (4) Cavazzana-Calvo, M.; Hacein-Bey, S.; de Saint Basile, G.; Gross, F.; Yvon, E.; Nusbaum, P.; Selz, F.; Hue, C.; Certain, S.; Casanova, J.-L. Gene therapy of human severe combined immunodeficiency (SCID)-X1 disease. *Science* **2000**, *288*, 669–672.
- (5) Marshall, E. Gene therapy on trial. *Science* **2000**, *288*, 951–957.
- (6) Check, E. Gene therapy: a tragic setback. *Nature* **2002**, *420*, 116–118.
- (7) Morrissey, D. V.; Lockridge, J. A.; Shaw, L.; Blanchard, K.; Jensen, K.; Breen, W.; Hartsough, K.; Machemer, L.; Radka, S.; Jadhav, V. Potent and persistent in vivo anti-HBV activity of chemically modified siRNAs. *Nat. Biotechnol.* **2005**, *23*, 1002–1007.
- (8) Xu, Z. P.; Zeng, Q. H.; Lu, G. Q.; Yu, A. B. Inorganic nanoparticles as carriers for efficient cellular delivery. *Chem. Eng. Sci.* **2006**, *61*, 1027–1040.
- (9) Wong, S. Y.; Pelet, J. M.; Putnam, D. Polymer systems for gene delivery—past, present, and future. *Prog. Polym. Sci.* **2007**, *32*, 799–837.
- (10) Maury, B.; Gonçalves, C.; Tresset, G.; Zeghal, M.; Cheradame, H.; Guégan, P.; Pichon, C.; Midoux, P. Influence of pDNA availability on transfection efficiency of polyplexes in non-proliferative cells. *Biomaterials* **2014**, *35*, 5977–5985.
- (11) Abdelhady, H. G.; Allen, S.; Davies, M. C.; Roberts, C. J.; Tendler, S. J.; Williams, P. M. Direct real-time molecular scale visualisation of the degradation of condensed DNA complexes exposed to DNase I. *Nucleic Acids Res.* **2003**, *31*, 4001–4005.
- (12) Lechardeur, D.; Sohn, K.; Haardt, M.; Joshi, P.; Monck, M.; Graham, R.; Beatty, B.; Squire, J.; O'brodovich, H.; Lukacs, G. Metabolic instability of plasmid DNA in the cytosol: a potential barrier to gene transfer. *Gene Ther.* **1999**, *6*, 482–497.
- (13) Schaffer, D. V.; Lauffenburger, D. A. Optimization of cell surface binding enhances efficiency and specificity of molecular conjugate gene delivery. *J. Biol. Chem.* **1998**, *273*, 28004–28009.
- (14) Chittimalla, C.; Zammut-Italiano, L.; Zuber, G.; Behr, J.-P. Monomolecular DNA nanoparticles for intravenous delivery of genes. *J. Am. Chem. Soc.* **2005**, *127*, 11436–11441.
- (15) Owens, D. E.; Peppas, N. A. Opsonization, biodistribution, and pharmacokinetics of polymeric nanoparticles. *Int. J. Pharm.* **2006**, *307*, 93–102.
- (16) Jang, J.-H.; Shea, L. D. Intramuscular delivery of DNA releasing microspheres: microsphere properties and transgene expression. *J. Controlled Release* **2006**, *112*, 120–128.
- (17) Kasturi, S. P.; Sachaphibulkij, K.; Roy, K. Covalent conjugation of polyethylenimine on biodegradable microparticles for delivery of plasmid DNA vaccines. *Biomaterials* **2005**, *26*, 6375–6385.
- (18) Bielinska, A. U.; Kukowska-Latallo, J. F.; Baker, J. R. The interaction of plasmid DNA with polyamidoamine dendrimers: mechanism of complex formation and analysis of alterations induced in nuclease sensitivity and transcriptional activity of the complexed DNA. *Biochim. Biophys. Acta - Gene Struct. Express.* **1997**, *1353*, 180–190.
- (19) Tresset, G.; Cheong, W. C. D.; Lam, Y. M. *J. Phys. Chem. B* **2007**, *111*, 14233–14238.
- (20) Ando, S.; Putnam, D.; Pack, D. W.; Langer, R. PLGA microspheres containing plasmid DNA: preservation of supercoiled DNA via cryopreparation and carbohydrate stabilization. *J. Pharm. Sci.* **1999**, *88*, 126–130.
- (21) Oster, C.; Kim, N.; Grode, L.; Barbu-Tudoran, L.; Schaper, A.; Kaufmann, S.; Kissel, T. Cationic microparticles consisting of poly(lactide-co-glycolide) and polyethylenimine as carriers systems for parental DNA vaccination. *J. Controlled Release* **2005**, *104*, 359–377.
- (22) Li, D.; Wagner, N. J. Universal binding behavior for ionic alkyl surfactants with oppositely charged polyelectrolytes. *J. Am. Chem. Soc.* **2013**, *135*, 17547–17555.
- (23) Yeo, L. Y.; Chang, H. C.; Chan, P. P.; Friend, J. R. Microfluidic devices for bioapplications. *Small* **2011**, *7*, 12–48.
- (24) Khan, I. U.; Serra, C. A.; Anton, N.; Vandamme, T. Microfluidics: A focus on improved cancer targeted drug delivery systems. *J. Controlled Release* **2013**, *172*, 1065–1074.
- (25) Valencia, P. M.; Farokhzad, O. C.; Karnik, R.; Langer, R. Microfluidic technologies for accelerating the clinical translation of nanoparticles. *Nat. Nanotechnol.* **2012**, *7*, 623–629.
- (26) Kim, C. S.; Duncan, B.; Creran, B.; Rotello, V. M. Triggered nanoparticles as therapeutics. *Nano Today* **2013**, *8*, 439–447.
- (27) Marre, S.; Jensen, K. F. Synthesis of micro and nanostructures in microfluidic systems. *Chem. Soc. Rev.* **2010**, *39*, 1183–1202.
- (28) Qi, A.; Chan, P.; Ho, J.; Rajapaksa, A.; Friend, J.; Yeo, L. Template-free synthesis and Encapsulation technique for layer-by-layer polymer nanocarrier fabrication. *ACS Nano* **2011**, *5*, 9583–9591.
- (29) Belliveau, N. M.; Huft, J.; Lin, P. J.; Chen, S.; Leung, A. K.; Leaver, T. J.; Wild, A. W.; Lee, J. B.; Taylor, R. J.; Tam, Y. K. Microfluidic synthesis of highly potent limit-size lipid nanoparticles for in vivo delivery of siRNA. *Mol. Ther.* **2012**, *1*, e37.
- (30) Kim, Y.; Lee Chung, B.; Ma, M.; Mulder, W. J.; Fayad, Z. A.; Farokhzad, O. C.; Langer, R. Mass production and size control of lipid-polymer hybrid nanoparticles through controlled microvortices. *Nano Lett.* **2012**, *12*, 3587–3591.
- (31) Kim, Y.; Fay, F.; Cormode, D. P.; Sanchez-Gaytan, B. L.; Tang, J.; Hennessy, E. J.; Ma, M.; Moore, K.; Farokhzad, O. C.; Fisher, E. A. Single step reconstitution of multifunctional high-density lipoprotein-derived nanomaterials using microfluidics. *ACS Nano* **2013**, *7*, 9975–9983.
- (32) Hong, J. S.; Stavis, S. M.; DePaoli Lacerda, S. H.; Locascio, L. E.; Raghavan, S. R.; Gaitan, M. Microfluidic directed self-assembly of liposome-hydrogel hybrid nanoparticles. *Langmuir* **2010**, *26*, 11581–11588.
- (33) Jahn, A.; Stavis, S. M.; Hong, J. S.; Vreeland, W. N.; DeVoe, D. L.; Gaitan, M. Microfluidic mixing and the formation of nanoscale lipid vesicles. *ACS Nano* **2010**, *4*, 2077–2087.
- (34) Tresset, G.; Iliescu, C. Electrical control of loaded biomimetic femtoliter vesicles in microfluidic system. *Appl. Phys. Lett.* **2007**, *90*, 173901.
- (35) Rondeau, E.; Cooper-White, J. J. Biopolymer microparticle and nanoparticle formation within a microfluidic device. *Langmuir* **2008**, *24*, 6937–6945.
- (36) Dashtimoghadam, E.; Mirzadeh, H.; Taromi, F. A.; Nyström, B. Microfluidic self-assembly of polymeric nanoparticles with tunable compactness for controlled drug delivery. *Polymer* **2013**, *54*, 4972–4979.
- (37) Majedi, F. S.; Hasani-Sadrabadi, M. M.; Emami, S. H.; Taghipoor, M.; Dashtimoghadam, E.; Bertsch, A.; Moaddel, H.; Renaud, P. Microfluidic synthesis of chitosan-based nanoparticles for fuel cell applications. *Chem. Com.* **2012**, *48*, 7744–7746.
- (38) Karnik, R.; Gu, F.; Basto, P.; Cannizzaro, C.; Dean, L.; Kyei-Manu, W.; Langer, R.; Farokhzad, O. C. Microfluidic platform for controlled synthesis of polymeric nanoparticles. *Nano Lett.* **2008**, *8*, 2906–2912.
- (39) Knight, J. B.; Vishwanath, A.; Brody, J. P.; Austin, R. H. Hydrodynamic focusing on a silicon chip: mixing nanoliters in microseconds. *Phys. Rev. Lett.* **1998**, *80*, 3863–3866.
- (40) Lim, J.-M.; Bertrand, N.; Valencia, P. M.; Rhee, M.; Langer, R.; Jon, S.; Farokhzad, O. C.; Karnik, R. Parallel microfluidic synthesis of size-tunable polymeric nanoparticles using 3D flow focusing towards *in vivo* study. *Nanomed.-Nanotechnol. Biol. Med.* **2014**, *10*, 401–409.
- (41) Tresset, G.; Marculescu, C.; Salonen, A.; Ni, M.; Iliescu, C. Fine control over the size of surfactant-polyelectrolyte nanoparticles by hydrodynamic flow focusing. *Anal. Chem.* **2013**, *85*, 5850–5856.

- (42) Johnson, B. K.; Prud'homme, R. K. Mechanism for rapid self-assembly of block copolymer nanoparticles. *Phys. Rev. Lett.* **2003**, *91*, 118302.
- (43) Rudorf, S.; Rädler, J. O. Self-Assembly of stable monomolecular nucleic acid lipid particles with a size of 30 nm. *J. Am. Chem. Soc.* **2012**, *134*, 11652–11658.
- (44) Tyn, M. T.; Calus, W. F. Temperature and concentration dependence of mutual diffusion coefficients of some binary liquid systems. *J. Chem. Eng. Data* **1975**, *20*, 310–316.
- (45) Trabelsi, S.; Raspaud, E.; Langevin, D. Aggregate formation in aqueous solutions of carboxymethylcellulose and cationic surfactants. *Langmuir* **2007**, *23*, 10053–10062.
- (46) Weigl, B. H.; Yager, P. Microfluidic diffusion-based separation and detection. *Science* **1999**, *283*, 346–347.
- (47) Castillo-León, J.; Rodríguez-Trujillo, R.; Gauthier, S.; Jensen, A. C.; Svendsen, W. E. Micro-“factory” for self-assembled peptide nanostructures. *Microelectron. Eng.* **2011**, *88*, 1685–1688.
- (48) Iliescu, C.; Taylor, H.; Avram, M.; Miao, J.; Franssila, S. A practical guide for the fabrication of microfluidic devices using glass and silicon. *Biomicrofluidics* **2012**, *6*, 016505.
- (49) Iliescu, C.; Tresset, G.; Xu, G. Continuous field-flow separation of particle populations in a dielectrophoretic chip with three dimensional electrodes. *Appl. Phys. Lett.* **2007**, *90*, 234104.
- (50) Iliescu, C.; Tresset, G.; Xu, G. Dielectrophoretic field-flow method for separating particle populations in a chip with asymmetric electrodes. *Biomicrofluidics* **2009**, *3*, 044104.